CHARACTERIZATION OF DEVONIAN SHALES WITH X-RAY COMPUTED TOMOGRAPHY

A. Ted Watson and Jim Mudra
Texas A&M University

1 Introduction

The Devonian shales of the eastern United States are considered a major potential source of future natural gas production, containing an estimated 1860 to 2580 trillion standard cubic feet of gas [1,2]. While natural gas has been produced from the shales since the 1820's, only an estimated 2.5 Tscf of gas had been produced through 1980 [3]. One key factor that has hindered more substantial production from the shales is that the tight shale rock has very low matrix permeability, so extensive natural or induced fractures may be required to obtain economic rates of gas production. Another factor is that a substantial quantity of gas may be stored in a fluid state other than as "free" gas in the pore space and may not be so readily identified or produced with conventional methods [4]. Presently, the manner of storage and transport in the shales is not well understood; this has hindered the development of reliable methods for exploration and production in the Devonian shales.

One problem in studying the shales is that conventional core tests on reservoir core samples simply do not work well. Special equipment or procedures are required to determine the permeabilities and porosities as low as those encountered in the shales [5]. However, a more fundamental problem is the very heterogeneous nature of the shales. A core sample may contain extremely low permeability matrix (with permeabilities of micro- or even nanodarcies [5]) but also contain fractures or other features that have permeabilites many orders of magnitudes higher. The presence and orientation of such high permeability features can have profound effects on the permeability that would be observed in a conventional test. Such an "averaged" value may not be very useful in describing reservoir behavior.

In this paper we report the use of X-ray computed tomography (CT) for investigating basic properties of Devonian shales. Unlike conventional experiments, CT imaging provides the means for detecting properties at various locations throughout the core sample. Of particular interest is the utility of the CT scanner for detecting microfractures and for quantitative determination of gas storage. When combined with other petrophysical experiments X-ray CT scanning can provide significant new information concerning the manner in which gas is transported and stored in the shales.

2 Theory

With CT scanning linear attenuation coefficients corresponding to small regions represented by voxels are determined. These are normally expressed on a standardized scale as CT numbers. The attenuation coefficient depends on the density and the atomic number of the material, as well as the energy of the X-ray source [6]. CT images from a single scan do not provide measures that are of immediate use for determining basic porous media properties, although they can provide a qualititative indication of density. However, multiple scans with

different saturating fluids can provide quantitative estimates of porosity and saturations [6-8].

Moss et al. [8] demonstrated quantitative determination of porosity using a dual scan method. Using xenon gas as a contrast agent with image subtraction techniques, they determined porosity images for conventional core samples and samples that exhibited dual porosity features. Our experiments will be carried out in a similar manner to those reported by Moss et al. However, a consideration in our experiments is that xenon in the shale sample may not exist simply as a gas with the same properties as a bulk gaseous phase. It is believed that natural gas may exist as an adsorbed [9] or perhaps densified [10] phase on clay or other mineral surfaces and that significant amounts may be in solution in the kerogen or other hydrocarbons [9,11]. Other gases, such as xenon, would behave in a similar fashion. The CT experiments can be used to determine the total amount of the saturating material contained or "stored" within the porous medium, irrespective of the fluid state.

Scans of the core sample after exposure to xenon gas and the evacuated core sample can be used to determine the amount of xenon contained in the regions corresponding to the voxels. Since the attenuation coefficient for the scan of the core sample with xenon as a saturating medium is the linear combination of the contributions from the xenon and rock, the attenuation coefficient for the xenon in the porous media (μ_x) can be obtained by differencing (on a voxel by voxel basis) the two images. The attenuation coefficient for the bulk xenon gas (μ_g) at the pressure and temperature for which the experiment is conducted can be obtained independently, such as by differencing the scans of the xenon filled and evacuated pressure vessel. We will define the ratio of these two coefficients to be the storage:

$$\mathcal{S} = \frac{\mu_x}{\mu_g}. \tag{1}$$

We next show how the storage can be used to determine the amount of xenon within any region corresponding to a voxel.

The attenuation coefficent for a pure substance can be related to an intrinsic property of the molecule [12]:

$$\mu_i = \frac{\sigma_i N_a}{M} \frac{m_i}{V} \tag{2}$$

where σ_i is the cross section of the absorption per molecule of component i, N_a is Avagadro's number, m_i is the mass of component i, V is the volume of a voxel, and M is the atomic mass. Using Eq. 2, the ratio of the attenuation coefficient for xenon in a voxel to that for xenon gas can be expressed as a ratio of mass densities:

$$\frac{\mu_x}{\mu_g} = \frac{\rho_x}{\rho_g}. \tag{3}$$

The density of xenon gas can be measured or determined with an appropriate equation of state. The amount of xenon in a region corresponding to a voxel can be determined by multiplying the storage by the density of xenon gas and the volume of the voxel. Note that if the xenon in the porous media exists in the same fluid state as xenon gas at the temperature and pressure of the experiment, the storage is equivalent to the porosity. If there is enhaced storage, such as by adsorption, solution, or densification, the storage will exceed the porosity.

3 Experiments

The experiments were conducted at Texaco EPDT on a fourth generation Technicare 2060 CT scanner. The scan time ranges from 2 to 8 seconds. Image array size is 512 x 512 with each pixel representing a volume element 0.25mm x 0.25mm x 2.0mm in size.

All the experiments were conducted at room temperature. A thin-walled aluminum pressure vessel 1.5 inches in diameter was used. Initial scans of the evacuated and xenon-filled pressure vessel were conducted to establish the attenuation coefficient for xenon gas as a function of pressure. The core sample was inserted into the pressure vessel. No confining pressure was used, and when gas was introduced, it could enter the core from any surface. The pressure vessel was first evacuated and scanned. Then, xenon gas was introduced into the pressure vessel. The pressure was maintained at 50 psia. A number of scans were taken at a single position selected in advance. Initially, scans were taken every minute. Later, they were taken more infrequently. At various times, scans were taken at succesive slices along the core sample.

The results presented in this paper were obtained using a sample of the Cleveland Shale from the Ashland Exploration Company E. J. Evans No. 91, located in Breathitt County, Kentucky. A 1.5 inch plug was cut perpendicular to the original 4 inch core sample. The sample is an organic-rich black shale.

4 Results and Discussion

Images of CT number for the evacuated core are shown in Figure 1. The slices are 2 mm thick, and there is 2 mm between slices. The lighter areas correspond to higher CT numbers, which indicates areas of greater density. Several regions of high density material that are roughly spherical are seen in slices 1–3 and 14–15. The regions are suspected to be pyrite nobules. A high density region which is most noticeable in the first five or six slices goes almost through the center of the core. There is also a high density region on the left of the core in slices 5–16. There are a number of thin low density regions that appear to be fractures which are most apparent in the first eight slices.

The third slice was chosen for the most detailed observation in the dynamic experiment. A series of images of the storage is shown for various times in Figure 2 (time is in seconds). The lighter areas correspond to regions of greater xenon storage. After a minute, the nobule has already shown significant xenon storage. After several minutes, the more permeable regions are identified as those for which there is obviously xenon storage. Most of these occur as parallel streaks; they were positively identified to be fractures by thin section analysis. There is one fracture in the left-center of the core that is perpendicular to these fractures. Throughout the experiment, the nobule in the upper left-hand part of the image remains distinct as a region of high xenon storage.

The experiment was concluded after 117 hours. Images of the storage for slices throughout the sample corresponding to the final time of the experiment are shown in Figure 3. They illustrate that a number of the high storage regions extend through a number of slices. For example, a vertical fracture on the left side of the third slice can be seen to go all the way through the plug. There is another fracture which can just be seen at the extreme left hand point of the third slice that can also be followed through the rest of the plug.

The value obtained for the storage greatly exceeds the porosity. A porosity value of 6.3% was measured for an adjoining sample [13]. The average storage for the third slice, as a function of time, is shown in Figure 4. Even though the experiment was conducted for more

than four days, the sample is continuing to take on xenon. The storage distribution was further analyzed by determining average storage values corresponding to selected regions within the core. Six regions with relatively high storage were selected as shown in Figure 5. Four regions (not shown here) with relatively low storage that corresponded to the dark areas were also selected. The average storage values for these regions are shown in Table 1. While about a quarter of the slice (by area) had a storage of only 1.3%, about a quarter of the slice had an average storage of 25%. Contributing factors to the excess storage as compared to the porosity are fractures that apparently were made during the the coring process, and the relatively large storage associated with the pyrite nobule. It does appear that significant amounts of xenon are stored in regions of the matrix that are adjacent to fractures. This would be consistent with a medium that has extremely low matrix permeability, but significant adsorption capabilities.

The relative adsorption properties of methane and xenon in these systems are not known. The molecular diameters are very nearly the same, and the molecular polarizability of xenon is intermediate to that of methane and ethane [14]. Schettler [15] has suggested that the molecular polarizability is a strong determinant of the adsorption isotherm slope. Based on this information, we might expect xenon to have similar adsorption properties to that of methane, or perhaps be a somewhat greater adsorbate.

A thin section was prepared from material within or near the third slice. A copy of a photograph of the thin section is shown in Figure 6. The nobule was identified as pyrite [16]. There is a very small fracture that connects the nobule to the outside of the sample; this evidently was the reason that xenon was detected there so early in the dynamic experiment. The central section of the thin section which appears light in Figure 6 was identified as a thin bed of argillaceous siltstone [16]. This region was identified as being relatively more dense from the CT scans of the evacuated core shown in Figure 1 (please note that the the thin section image is offset by about 80° compared to the CT images). Most of the various regions that were seen to be particularly permeable in the dynamic experiments were identified to be fractures. The lack of any appreciable mineralization within these fractures suggested that they were most probably not naturally occuring fractures [16]. It is suspected that these were induced in the coring process. Reflected fluorescent light petrography and scanning electron microscopy were used to examine the presence of microporosity. Generally, significant matrix microporosity was not detected in any portion of the sample [16].

The relative size of fracture that could be detected by the CT scanner was quite small. Virtually all the fractures seen in the thin section could also be detected from the CT images. Based on measures from the thin section, the large fractures appear to be of the order of 100 microns, and the smaller ones appear to be a few tens of microns. There is a fracture that runs from left to right through the center of the thin section. This is barely discernible from the thin section, and so small that a reasonable estimate of size is not available. But this fracture is clearly discernible in the CT image corresponding to the final time in the dynamic experiment (see Figure 2). Thus, fractures which are considerably smaller than the resolution of the instrument can be detected. One factor which enhances the ability to detect fractures is the great constrast between storage values for voxels for regions that contain a fracture compared to the very small storage associated with the matrix region. Another factor is that the relatively great storage that seems to occur in the vicinity of the fractures results in an amount of xenon which is much greater than that which occupies the fracture.

5 Conclusions

1. The use of a dual-scan X-ray CT method for quantitative determination of storage in a Devonian shale sample was demonstrated.

2. Fractures considerably smaller than the resolution of the instrument were detected.

3. Observations of the distribution and magnitude of storage are consistent with a medium of very small permeability and large adsorption.

4. Pyrite nobules were identified as regions of high gas storage.

6 Acknowledgements

The authors thank Lorne Davis, Greg Pepin, Robert Moss, and other members of the Petrophysics Department at Texaco EPTD for their help with the CT scanning and image analysis. The efforts of Pat Lowry of K&A Energy Consultants in the petrophysical analyses and the partial support of this work by the Gas Research Institute are also gratefully acknowledged.

7 References

1. National Petroleum Council, *Unconventional gas resources: Volume III, Devonian Shale*, Washington, D. C. (1980).

2. Zielinski, R.E. and R.D. McIver, *Resource and exploration assessment of the oil and gas potential in the Devonian Shales of the Appalachian Basin*, DOE/DP/0053-1125, Miamisburg, OH, Mound Laboratories (1982).

3. Schrider, L.A. and R.L. Wise, "Potential New Sources of Natural Gas," *J. Pet. Tech.* 32 (4) 703 (1980).

4. Lane, H.S., D.E. Lancaster, and A.T. Watson, "Characterizing the Role of Desorption in Gas Production from Devonian Shales," *Energy Sources*, 13 (3) 337 (1991).

5. Soeder D.J., "Porosity and Permeability of Eastern Devonian Gas Shale," *SPE Form. Eval.* 3 (1) 116 (1988).

6. Vinegar, H.J. and S.L. Wellington, "Tomographic imaging of three-phase flow experiments," *Rev. Sci. Instrum.* 58 (1) 96 (1987).

7. Withjack, E.M. "Computed Tomography for Rock-Property Determination and Fluid-Flow Visualization," *SPE Form. Eval.* 3 (4) (1988).

8. Moss, R.M., G.P. Pepin, and L.A. Davis, "Direct Measurement of the Consituent Porosities in a Dual Porosity Matrix," SCA Conference Paper Number 9003, August (1990).

9. Schettler, P.D., C.R. Parmely, and W.J. Lee, "Gas Transport and Storage in the Devonian Shales," *SPE Form. Eval.* 4 (3) 371 (1989).

10. Kim, M.J., K.R. Hall, J.C. Holste, and J.C. Slattery, "Van der Waals Adsorption of Supercritical Methane in Small Pores," submitted for publication to *J. of Colloid and Interface Science.*

11. Kuuskraa, V.A., D.E. Wicks, W.K. Sawyer, and P.R. Esposito, *Technically recoverable Devonian Shale gas in Ohio*, DOE/MC/19239-1525, Washington, D.C., Lewin and Associates, Inc. (1983).

12. Eisberg, R.M., *Fundamentals of Modern Physics*, Wiley, New York (1961).

13. Luffel, D.L. and F.K. Guidry, "Core Analysis Results, Comprehensive Study Wells, Devonian Shale," GRI Topical Report, July (1989).

14. Israelachvili, J.N., *Intermolecular and Surface Forces*, Academic Press (1985).

15. Schettler, P.D. and C.R. Parmely, "Gas Composition Shifts in Devonian Shales," *SPE Res. Eng.* 4 (3) 283 (1989).

16. Purrazzella, P.M., "Petrographic Analysis, Cleveland Shale, Ashland Exploration Company, E.J. Evans No. 91 Well, Breathitt County, Kentucky," Final Report, K&A Energy Consultants (1991).

Table 1. Analysis of Slice # 3

High Permeability Regions	Storage	Area (%)
1	0.34	2.0
2	0.29	5.2
3	0.19	5.8
4	0.20	2.5
5	0.23	7.6
6	0.29	1.1

Low Permeability Regions	Storage	Area (%)
1	0.023	4.5
2	0.005	7.8
3	0.005	7.8
4	0.025	6.6

Composite	Storage	Area (%)
High Permeability Regions	0.25	24
Low Permeabilty Regions	0.013	27
Remainder	0.18	49
Entire Slice	0.15	100

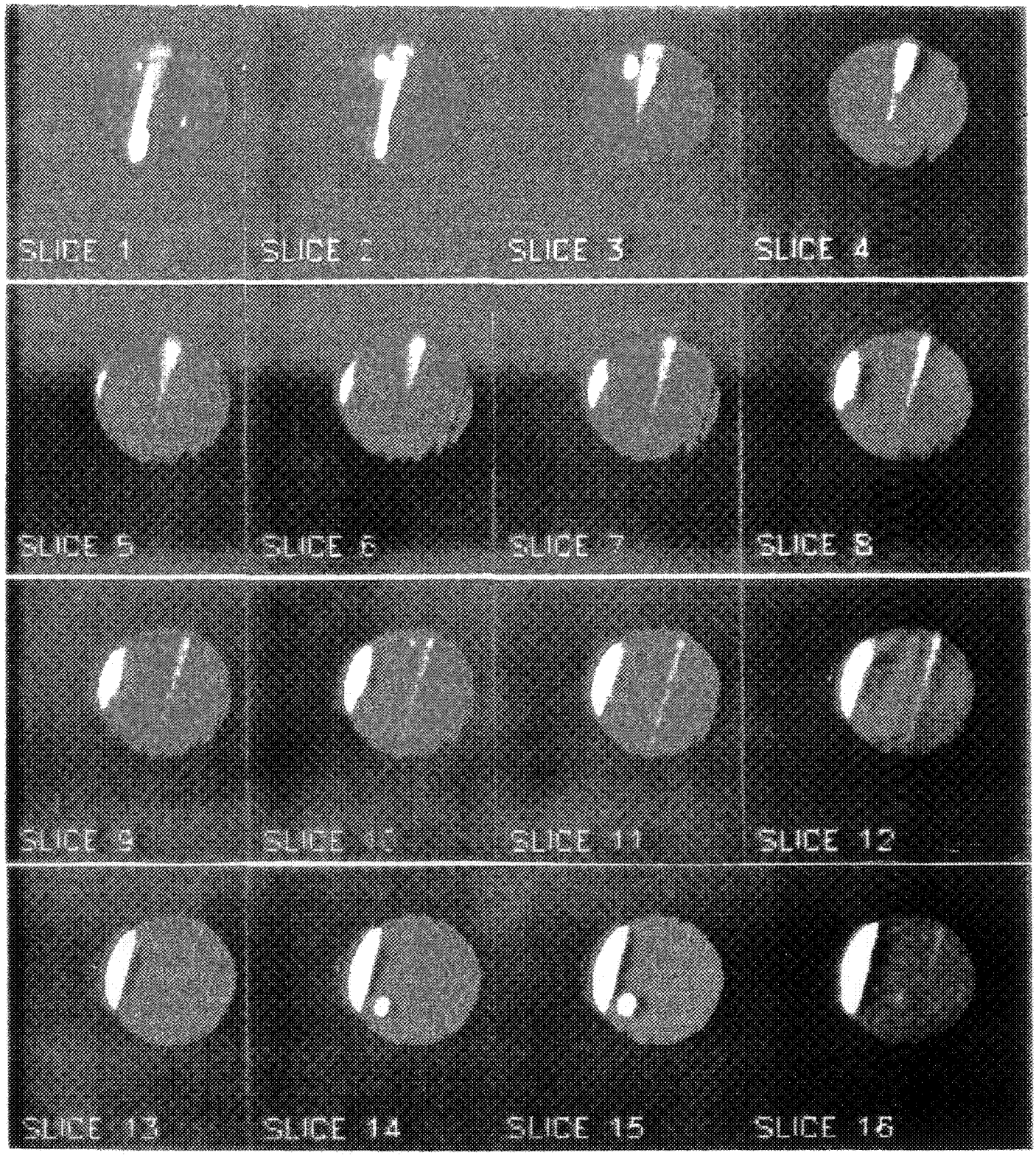

Figure 1. Images Of CT Number - Evacuated Core.

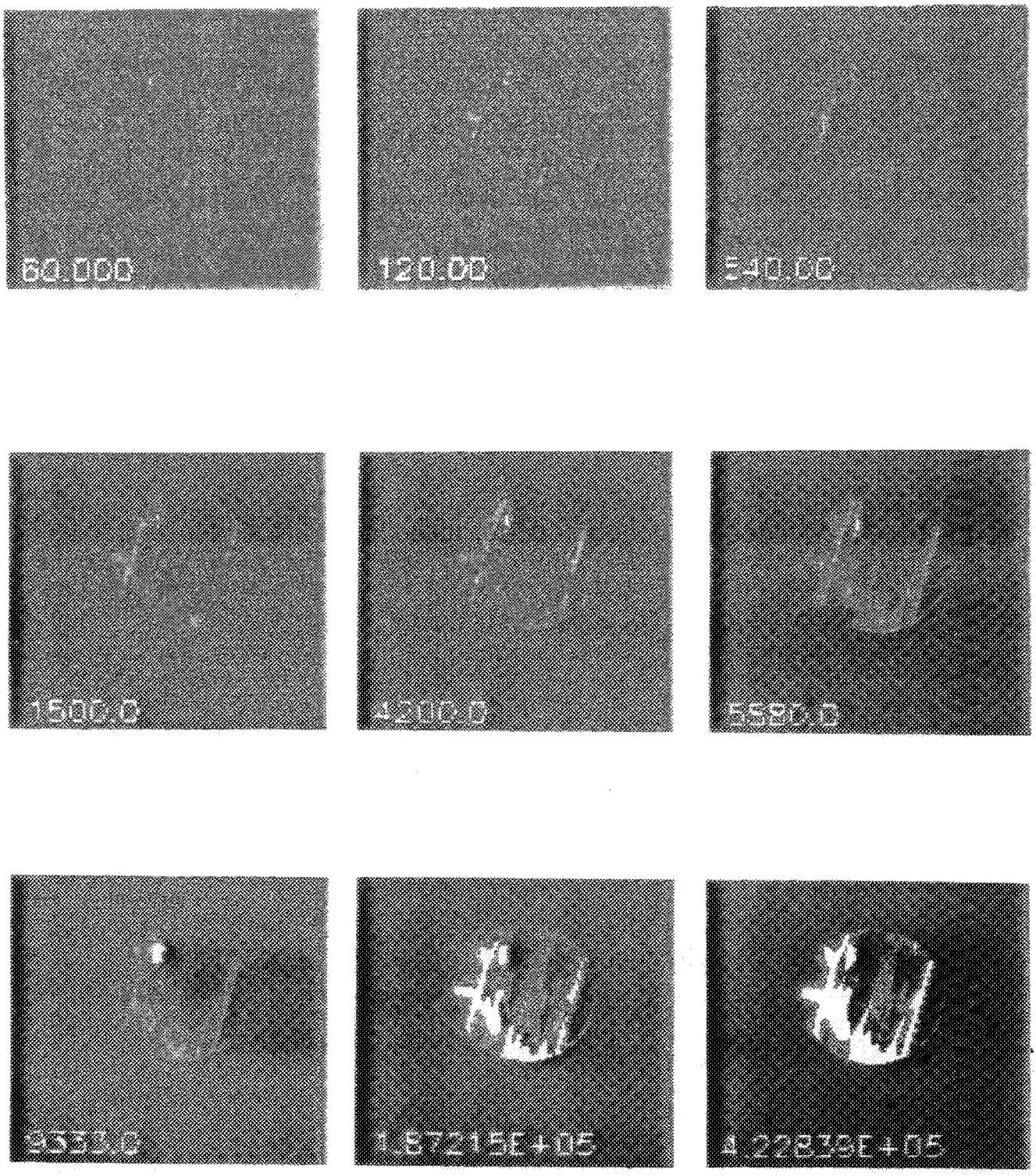

Figure 2. Storage Images In Dynamic Experiment - Slice No. 3.

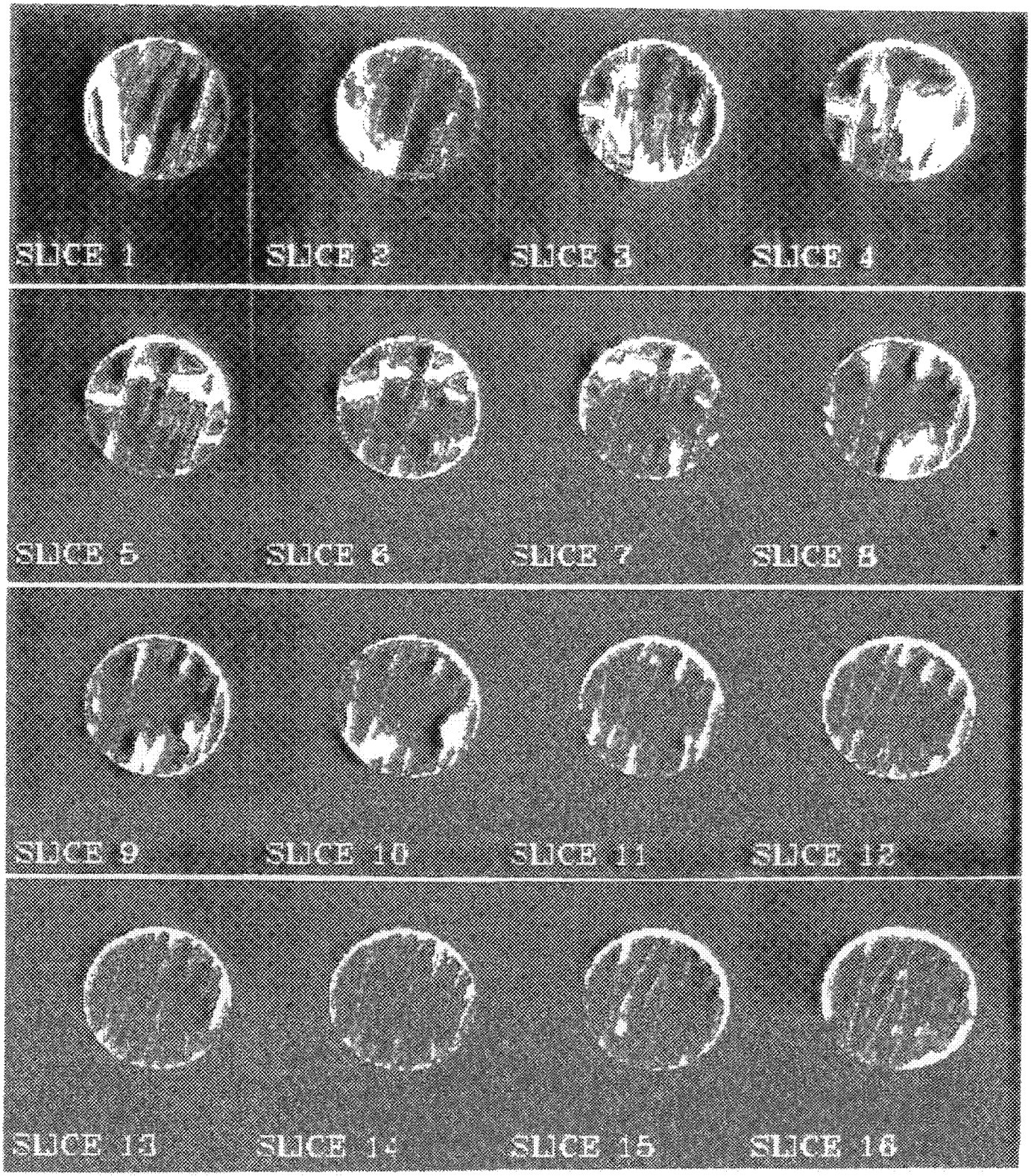

Figure 3. Storage Images - Final Experimental Time.

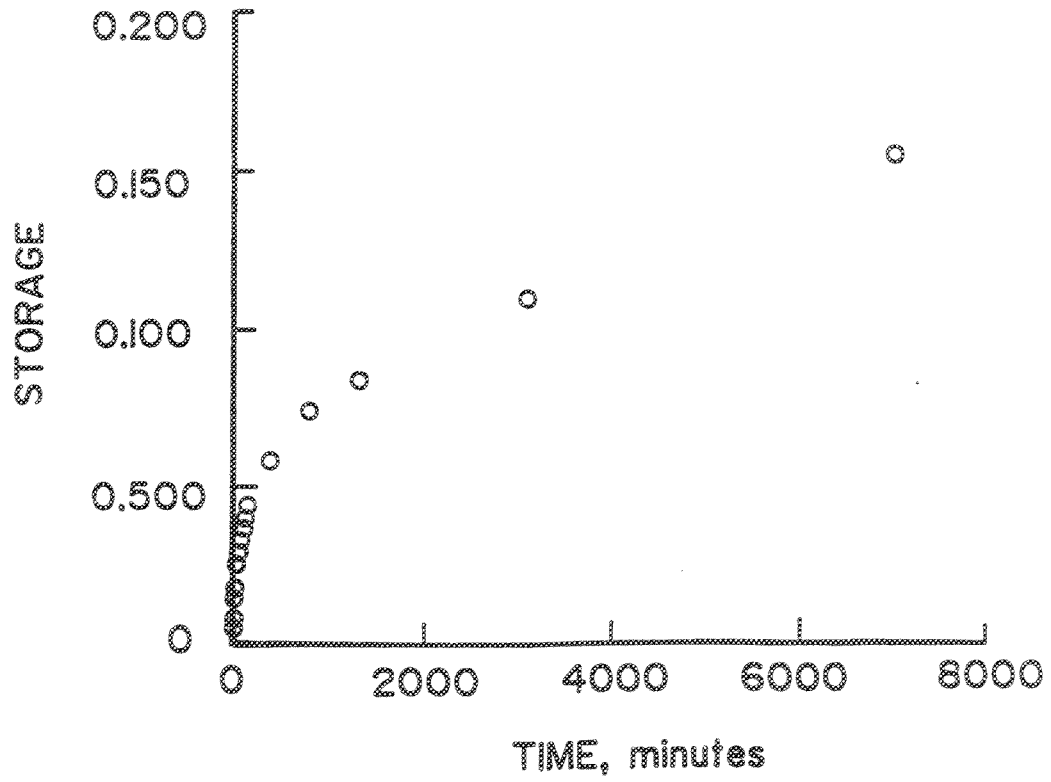

Figure 4. Storage In Slice No. 3.

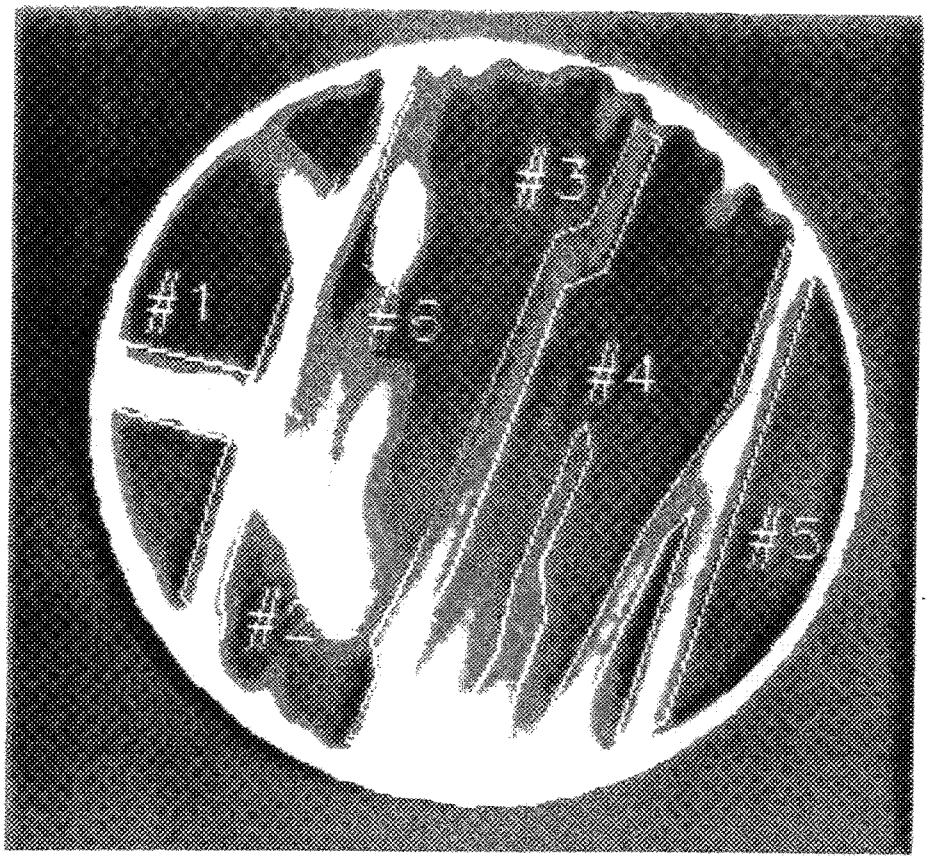

Figure 5. Selection Of High Storage Regions.

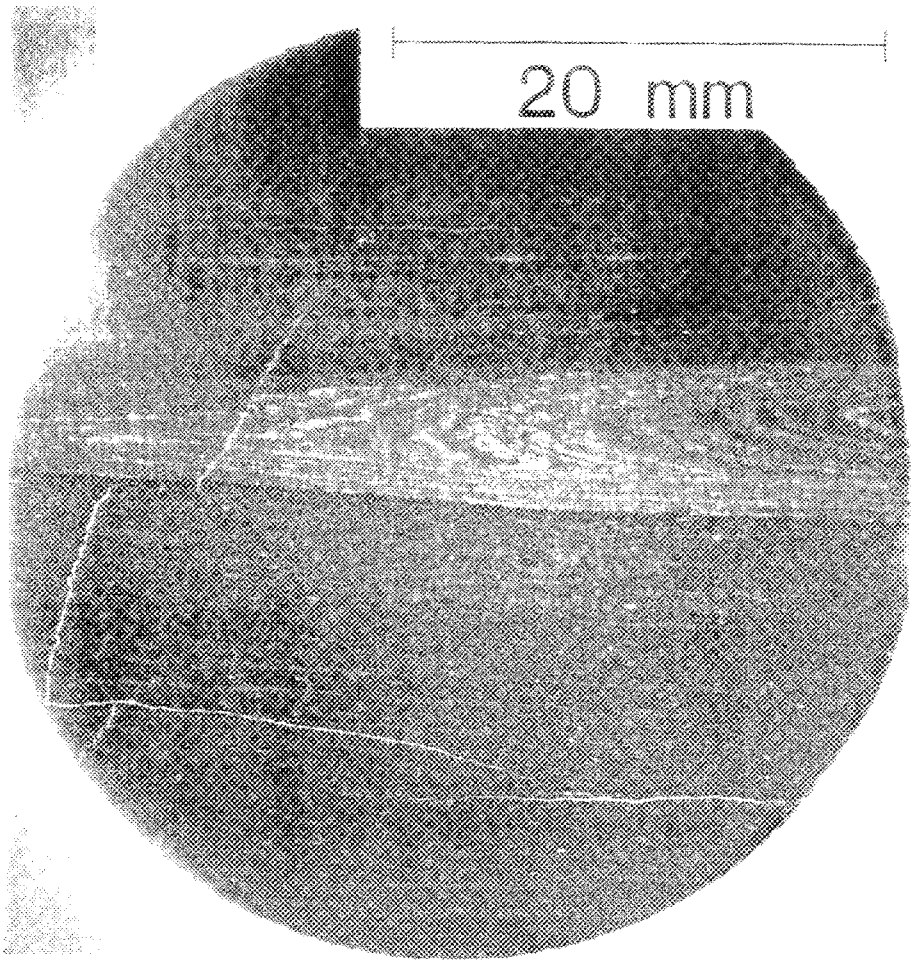

Figure 6. Photograph Of Thin Section Of Slice No. 3